Environmental Effects on Solar Array Electrostatic Discharge Current Waveforms and Test Results

Teppei Okumura,* Hirokazu Masui,† Kazuhiro Toyoda,‡ and Mengu Cho§
Kyushu Institute of Technology, Kitakyushu 804-8550, Japan
and
Kumi Nitta¶ and Mitsuru Imaizumi**
Japan Aerospace Exploration Agency, Tsukuba 305-8505, Japan

A solar array electrostatic discharge ground test is necessary to assure spacecraft reliability in orbit. Laboratory experiments were carried out to characterize an electrostatic discharge current waveform with different background pressures and charging environments to identify the importance of the test setup. The waveform strongly depended on the background pressure. This difference can affect the result of the solar cell degradation test. However, in the case of the secondary arc test, the difference of the primary arc current waveform did not affect the duration of the secondary arc. The current available from a power supply mostly determined the duration of the secondary, irrespective of the test environment. Methods to control the primary arc current supplied by an external capacitance are proposed.

Nomenclature

C_{BC}	=	bus capacitance, F
C_{ext}	=	external capacitance, F
C_p	=	current probe
C_1, C_2, C_3	=	capacitance to simulate the capacitance of the solar array, F
dP_{max}	=	change of maximum power due to a number of the primary arc, %
I_{peak}	=	peak of the primary arc current, A
I_{st}	=	string current, A
L_{ext}	=	external inductance, H
N_{arc}	=	number of the primary arc
N_e	=	plasma density, m^{-3}
P_{max}	=	maximum power of the solar cell, W
$P_{max_{after}}$	=	maximum power of the solar cell after the experiment, W
$P_{max_{before}}$	=	maximum power of the solar cell before the experiment, W
Q_{arc}	=	charge of the primary arc, C
R_{ext}	=	external resistance, Ω
R_{gs}	=	resistance on the discharge circuit, Ω
R_L	=	load resistance, Ω
T_{arc}	=	primary arc duration, s
T_e	=	electron temperature, eV
T_{end}	=	end time of the primary arc defined by time when the current becomes 10% of the peak values
T_1	=	start time of the primary arc, s
T_2	=	end time of the primary arc defined by time when the current becomes 5% of the peak values
V_b	=	bias voltage, V
V_p	=	voltage probe
V_{st}	=	string voltage; the potential difference between the string across the test gap, V
V_1, V_2	=	voltage power supply, V

I. Introduction

ELECTROSTATIC discharge (ESD) on a solar array panel is considered as the major cause of satellite or orbit anomaly [1]. The reliability of a spacecraft solar array needs to be confirmed thoroughly before its launch. There is an international collaboration effort among several countries on a project to establish an international standard of the solar array discharge test. To propose a proper test setup, the discharge phenomena should be understood correctly [2].

A cross-sectional view of a typical solar array is shown in Fig. 1. The boundary at which the insulator, conductor/semiconductor, and space meet is referred to as a triple junction. In geosynchronous orbit (GEO), the spacecraft encounters high-energy electrons during substorm, and the spacecraft potential becomes negative with respect to the ambient plasma. The coverglass surface can emit electrons due to secondary electron emission and photo electron emission. If the surface emits enough electrons, the potential of the coverglass surface becomes positive against the spacecraft. The potential gradient inside the coverglass is known as the inverted potential gradient.

In low Earth orbit (LEO), ionospheric plasma determines the spacecraft potential. Because of the difference in mobility of ions and electrons, the potential becomes negative against the ambient plasma. In LEO, the coverglass surface potential becomes positive with respect to the spacecraft chassis potential as ions collide on the coverglass surface. The inverted potential gradient is thus also generated in the LEO [3].

Although the charging process is different for GEO and LEO, a discharge occurs as the electric field concentrates near the triple junction for both of the orbits [3]. Once the discharge occurs on the solar array under the inverted potential gradient, a cathode spot is formed on the solar cell surface resembling a vacuum arc and the discharge is called a primary arc. The discharge plasma expands over the solar array surface and is called flashover plasma. The charged insulator material, such as coverglass, supplies electrostatic energy to the primary arc because the flashover plasma couples with the

*Postdoctoral Fellow, Department of Electric Engineering, 1-1 Sensui Tobata-ku; okumura@ele.kyutech.ac.jp.
†Postdoctoral Fellow, Department of Electric Engineering, 1-1 Sensui Tobata-ku; masui@ele.kyutech.ac.jp. Young Professional Member AIAA.
‡Associate Professor, Laboratories of Spacecraft Environment Engineering, 1-1 Sensui Tobata-ku; toyoda@ele.kyutech.ac.jp.
§Professor, Department of Electric Engineering, 1-1 Sensui Tobata-ku; cho@ele.kyutech.ac.jp. Senior Member AIAA.
¶Associate Senior Engineer, Spacecraft Power Systems Group, 2-1-1 Sengen Tsukuba; nitta.kumi@jaxa.jp.
**Associate Senior Engineer, Spacecraft Power Systems Group, 2-1-1 Sengen Tsukuba; imaizumi.mitsuru@jaxa.jp.
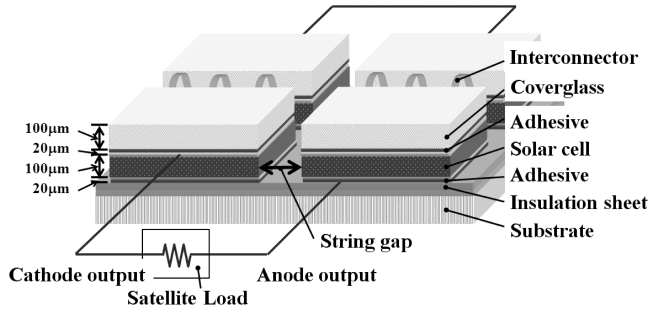
Fig. 1   Cross-sectional view of a typical solar array.

insulator. The primary arc degrades the solar cell [4,5] and triggers a secondary arc, which is explained in the following paragraph [6,7].

On a typical solar array, each solar cell can have a different potential from another solar cell located at the adjacent string across the string gap, as shown in Fig. 1. The generation voltage of the solar array determines the potential difference across the string gap. Many commercial satellites today generate their power at 100 V and the potential difference across the string gap potentially becomes 100 V. When the primary arc occurs at the string gap, low-resistive primary arc plasma can short the string gap. This short-circuit event is known as the secondary arc.

Although it is desired to simulate the orbit environment in the solar array discharge test as closely as we can, it is impossible to simulate completely the actual environment because of technical limitations and matters of cost effectiveness. Therefore, various experimental environments are used for the ground experiment: the background pressure is higher than that found in orbit and the charging mechanism of coverglass is not quite the same as that in orbit. If the environment does not affect the experimental result, then the nonrealistic environment does not pose a problem. Otherwise, the test method will have to be revised. The purpose of the present paper is to investigate how the test environment, such as the pressure and the charging mechanism, affects the test results.

In the second part of the paper, we describe the dependence of the primary arc current waveform on the test environment. The laboratory experiment by Matéo-Vélez et al. [8] showed that the current waveform depended on the distance between the arc inception point and the ground point forming the arc current circuit. In the present paper, we will carry out more detailed study about the effect of chamber background pressure on the current waveform.

In the third part, we examine the effect of the test environment on the solar cell degradation test. Matéo-Vélez et al. [8], Vayner et al. [9], and Okumura et al. [10] presented the results of the solar cell degradation test carried out in three different chambers but with identical solar cell coupons. In all three cases, the solar cells were degraded. In the present paper, we examine whether the solar cell degradation in a low-temperature-plasma environment differs from that in an energetic electron beam environment.

In the fourth part, we present the test result about whether the environment affects the secondary arc duration. A previous study carried out in Europe [11] compared the probability of the secondary arc inception between two different charging environments: energetic electron beam and low-temperature plasma. The two tests gave similar results when the energy provided by an external capacitance was kept the same. In the present paper, we investigate the effect of the charging environment on how long a secondary arc continues.

In the fifth part, we propose methods to control the primary arc current waveform. In the solar array ESD test, we need to make the primary arc current as flight-representative as possible. Although there has been no measurement of the arc current waveform done in orbit, four independent laboratory experimental studies [12–15] gave more or less the same waveform, which indicated that the primary arc current was provided by a flashover plasma expanding with a speed of 10 km/s to the extent of at least 2 m. In the present paper, we propose circuit setups to provide the primary arc current based on this state-of-art knowledge and verify their waveforms.

In the sixth part, we conclude the paper with suggestions of future works.

II.   Environmental Dependence of the Primary Arc Current Waveform

Solar cell samples for the primary arc test are shown in Fig. 2. One solar cell is the InGaP/GaAs/Ge solar cell (3J cell), and the other is a silicon solar cell with an integrated bypass function (Si cell). The solar cell is attached to an aluminum panel that is insulated by polyimide sheet. The coverglass is glued on top of each solar cell by transparent adhesive. The size of the coverglass/solar cell is 35 mm × 70 mm × 100 μm. In this section, the result of the primary arc test for the Si cell and 3J cell are discussed.

To investigate the effect of different test environments on the primary arc current waveform, three experiment facilities (namely, LEO, GEO, and PEO) and chamber A were used. In all of the chambers, the circuit setup for the primary arc test is the same, except the value of each circuit element. The circuit layout is shown in Fig. 3. This circuit is currently used in research institutes working on ESD tests [8–10]. The voltage power supply V_b simulates the spacecraft potential with respect to the ambient plasma. There are two energy sources for the primary arc current in orbit. One is a capacitance of the spacecraft body with respect to the ambient plasma, which is usually less than 1 nF. The capacitance is often called the absolute capacitance. The absolute capacitance is quickly discharged by the current between the arc inception point and the ambient plasma. Another source is a capacitance inherent to insulator on spacecraft surface. It is often called the differential capacitance. The majority of the differential capacitance comes from the coverglass on solar panel. In the orbit, the flashover plasma propagates over the solar array surface after the primary arc inception at the triple junction on solar array. The electrostatic charge stored in coverglass within the flashover plasma propagation area supplies the energy to the primary arc as the flashover plasma neutralizes the charge on the coverglass surface. Therefore, the energy of the primary arc depends on the plasma propagation area. In the ground test, because it is impossible for us to install the real size of the solar array inside the vacuum chamber, we use C_{ext} to simulate the missing coverglass of
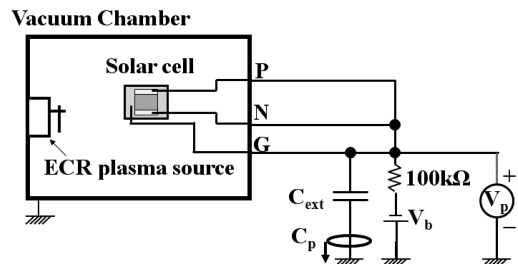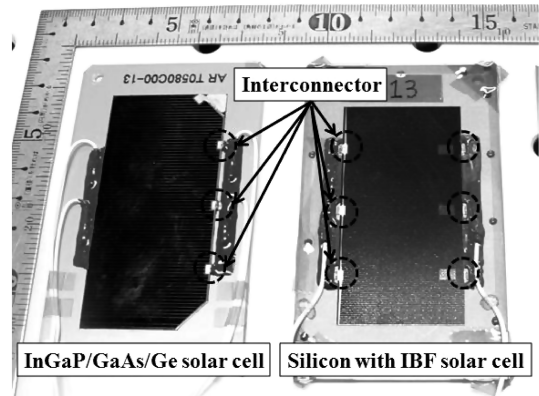

Fig. 2   Experimental sample.

Fig. 3   Discharge circuit for the primary arc test.

Table 1 Experimental conditions of chamber A, LEO chamber, and PEO chamber

Conditions	Chamber A				LEO chamber		PEO chamber
Pressure, Pa	5.0×10^{-4}	1.8×10^{-3}	3.9×10^{-3}	9.1×10^{-3}	5.3×10^{-3}	2.1×10^{-3}	2.7×10^{-3}
Gas flow	0.4 sccm	1.3 sccm	2.5 sccm	5 sccm	0.3 sccm	0.4 sccm	0.4 sccm
Electron temperature	0.9 eV	0.7 eV	0.7 eV	0.4 eV	1 eV	1 eV	1 eV
Plasma density	1.4×10^{11} m^{-3}	1.9×10^{11} m^{-3}	2.1×10^{11} m^{-3}	9.1×10^{11} m^{-3}	1×10^{12} m^{-3}	1×10^{12} m^{-3}	1×10^{12} m^{-3}
C_{ext}	500 nF	500 nF	500 nF	500 nF	500 nF	500 nF	470 nF
Bias voltage	-470 V	-530 V	-450 to -530 V	-400 to -480 V	-400 V	-400 V	-550 to -600 V
Chamber size		1 m diameter 1.4 m length				1 m diameter 1.2 m length	1 m diameter 1.2 m length

the solar array. The voltage waveform is measured by the voltage probe V_p. The current waveform is measured by the current probe C_p.

The size of chamber A is 1.4 m in length and 1 m in diameter. The shortest distance from the test sample to the chamber wall is 0.2 m. Chamber A is equipped with an electron cyclotron resonance (ECR) plasma source that generates Xe plasma. The gas flow rate to an ECR plasma source is changed to vary the background pressure. The pressure is measured by an ionization gauge. The gas flow rate, chamber pressure, plasma density, and electron temperature are listed in Table 1. The pressure is changed from 5.0×10^{-4} Pa to 9.1×10^{-3} Pa by varying the gas flow rate. The plasma density also changes with the gas flow rate. However, the change of plasma density is much smaller than the change of pressure.

The size of the LEO chamber is 1 m in diameter and 1.2 m in length. The shortest distance between the sample and the chamber wall is 0.4 m. The LEO chamber is also equipped with an ECR plasma source that generates Xe plasma to simulate a LEO plasma environment. It is equipped with two turbomolecular pumps to control the pressure. In this experiment, the pressure is 5.3×10^{-3} Pa with 0.3 sccm and 2.1×10^{-3} Pa with 0.4 sccm. The plasma density and electron temperature does not change with the pressure: $N_e = 1 \times 10^{12}$ m^{-3} and $T_e = 1$ eV.

The PEO chamber is almost identical to the LEO chamber. Its size is 1 m in diameter and 1.2 m in length. The shortest distance between the sample and the chamber wall is 0.4 m. The PEO chamber is also equipped with an ECR plasma source that generates Xe plasma to simulate a LEO plasma environment. A turbomolecular pump keeps the pressure around 2.7×10^{-3} Pa with 0.4 sccm during the experiment. The plasma density and electron temperature does not change with the pressure: $N_e = 1 \times 10^{12}$ m^{-3} and $T_e = 1$ eV.

In the case of the experiment in chamber A and the LEO chamber, C_{ext} is 500 nF. In the case of the experiment in the PEO chamber, C_{ext} is 470 nF. To control the number of arcs, V_b is changed from -400 to -600 V. The primary arc current waveform is measured by using a dc current probe (dc to 50 MHz). The voltage waveform is measured by a differential voltage probe (dc to 2500 MHz).

The GEO chamber is equipped with an electron beam gun to simulate the high-energy electron environment in GEO. The experimental environment in GEO is detailed in Table 2. To control the arc frequency, the current density of the electron beam gun is changed from 30 to 100 μA. In the case of the experiment in the GEO chamber, C_{ext} is 64.5 nF and V_b is -4 kV. The primary arc current waveform is measured by a dc current probe (dc to 50 MHz). The voltage waveform is measured by a differential voltage probe (dc to 75 MHz).

The primary arc current waveforms of the Si cell in chamber A for various background pressures are shown in Fig. 4. The primary arc current waveform in the case of 5.0×10^{-4} Pa has multiple peaks. However, for 1.8×10^{-3}, 3.9×10^{-3}, and 9.1×10^{-3} Pa, the primary arc current has one peak.

The primary arc current waveform of the Si cell in the LEO chamber for the two pressures and the primary arc current waveform of the Si cell in the GEO chamber are shown in Fig. 5. In the LEO chamber at 5.3×10^{-3} Pa, the primary arc current has a single peak. On the other hand, the primary arc current in the LEO chamber with lower pressure has multiple peaks. The primary arc current in the GEO chamber also has multiple peaks. From Figs. 4 and 5, it is seen

Table 2 Experimental condition of the GEO chamber

| Conditions	Values
Pressure	3×10^{-3} Pa
Acceleration voltage	4.5 kV
Beam current	30–100 μA
C_{ext}	65 nF
Bias voltage	-4 kV
Chamber size	0.6 m diameter, 0.9 m length

that the pressure and charging environment affect the primary arc current waveform.

The peak current of the primary arc is defined as I_{peak}. The times when the current is 5% of I_{peak} are defined as T_1 and T_2. The primary arc duration is defined as

$$T_{\text{arc}} = T_2 - T_1 \tag{1}$$

The charge amount of the primary arc current is described by

$$Q_{\text{arc}} = \int_{T_1}^{T_2} I(t)\,dt \tag{2}$$
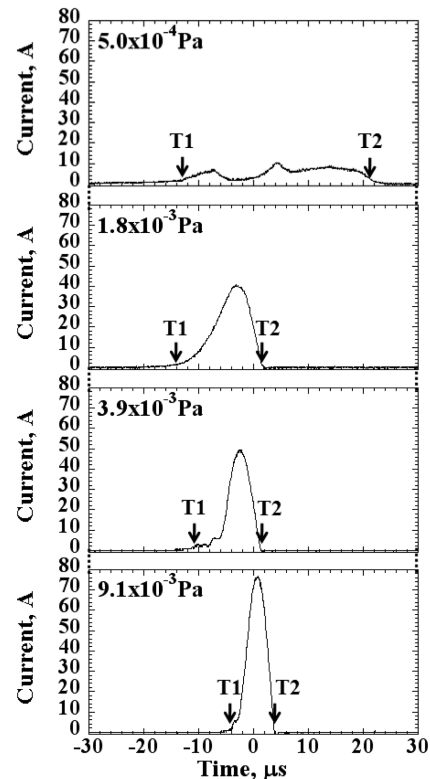
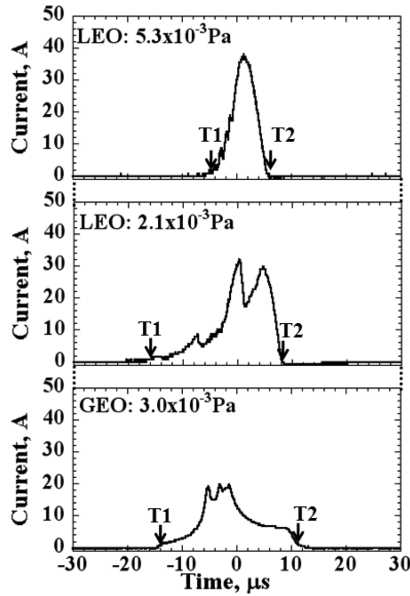**Fig. 4 Primary arc current waveform of the Si cell in chamber A for different pressures.**

Fig. 5 Primary arc current waveforms of the Si cell in the LEO chamber and GEO chamber.

Fig. 6 Primary arc current waveforms of the 3J cell in the LEO, PEO, and GEO chambers.

The peak of the primary arc current I_{peak}, the pulse duration T_{arc}, the amount of charge Q_{arc}, the bias voltage and the number of the primary arcs during experiment time N_{arc} are listed in Table 3. Each parameter is listed with standard deviation. Because the bias voltage was changed in the case of 3.9×10^{-3} Pa and 9.1×10^{-3} Pa in chamber A to control the arc frequency, the standard deviation of I_{peak} and Q_{arc} for the two cases is large. The standard deviation of T_{arc} is less than 10% throughout the four cases in chamber A. We can see that T_{arc} increases and I_{peak} decreases as the pressure decreases.

In the experiment in the LEO chamber, we cannot compare I_{peak} because the bias voltage was different. T_{arc} increases with decrease of pressure as it does in chamber A. The pressure is 3×10^{-3} Pa in the GEO chamber. Although Q_{arc} in the GEO chamber is comparable with Q_{arc} in the LEO chamber under the pressure of 5.3×10^{-3} Pa, the primary arc in the GEO chamber has smaller I_{peak} and larger T_{arc}. In contrast, Q_{arc} in the case of 2.1×10^{-3} Pa in the LEO chamber is slightly larger than Q_{arc} in the GEO chamber; however, T_{arc} is comparable.

The difference of the solar cell type may affect the primary arc current waveform, because the capacitance of the PN junction is determined by the solar cell type. Here, the primary arc current waveform of the 3J cell in the LEO, PEO, and GEO chambers are shown in Fig. 6. In the LEO chamber at 5.3×10^{-3} Pa, the primary arc current has a single peak. On the other hand, in the GEO chamber and PEO chamber, the primary arc current has multiple peaks. The pressure dependence on current waveform of the 3J cell is the same as the Si cell. The primary arc characteristics of the 3J cell are shown in Table 4. T_{arc} is decreasing with increasing of pressure. This fact shows that there is no significant effect of the solar cell type on the primary arc current waveform. In the discharge circuit in Fig. 3, the P electrode and N electrode are shorted: that is, there is not a potential difference between the P electrode and N electrode. Therefore, in the case of the discharge circuit in Fig. 3, we can ignore the difference of the solar cell type. In the case of the secondary arc test, which is
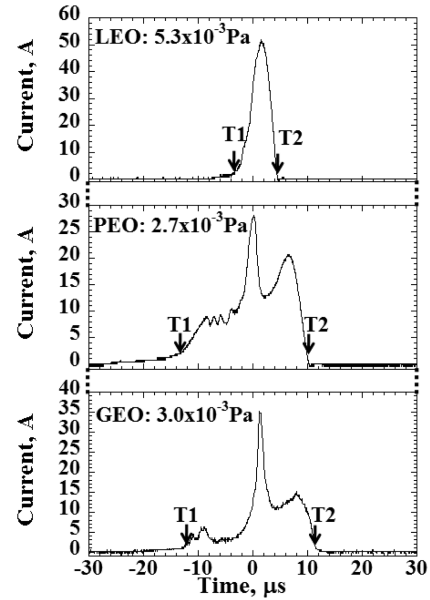
discussed in Sec. IV, because the electrodes of the solar cell do not short, the type of the solar cell may affect the waveform.

The plasma density can be roughly categorized into two ranges: one is 1.4×10^{11} to 2.1×10^{11} m^{-3} and the other is 9.1×10^{11} to 1×10^{12} m^{-3}. In the former range, the pressure varies from 5.0×10^{-4} to 3.9×10^{-3} Pa, a factor of 8. In the latter range, the pressure varies from 2.1×10^{-3} to 9.1×10^{-3} Pa, a factor of 4. With the same plasma density, as the pressure increases, the pulse duration decreases, as shown in Table 3. In Fig. 7, we can see the general trend of the decreasing pulse duration with the increasing pressure. The pulse duration is slightly different for the same pressure among the different chambers. The cause of this difference is considered to be the distance between the test sample and the chamber wall [8]. Therefore, the pressure is one of the important factors affecting the primary arc current waveform.

The term of *pressure* used in the present paper can be translated to *background neutral density*, as all of the experiments were done at room temperature. For the case of chamber A and the LEO chamber, the pressure is equivalent to xenon density. For the case of the GEO chamber, the pressure is equivalent to water vapor density. The capacitance and the resistance associated with the primary arc determine its duration. The higher the background density, the more ionization occurs between the arc inception point and the chamber wall, reducing the overall resistance of the primary arc circuit. Because we do not see much difference in the pulse duration between the GEO and LEO chambers, considering the difference of many orders of magnitude in the background plasma density, the primary arc resistance is mostly determined by ionization of the background neutral gas, not the ambient plasma existing before the arc inception.

III. Solar Cell Degradation Test

There are two purposes in a solar array ESD test. One is to characterize the primary arc phenomena, such as arc frequency and

Table 3 Primary arc current characteristics of the Si cell in chamber A, LEO chamber, and GEO chamber

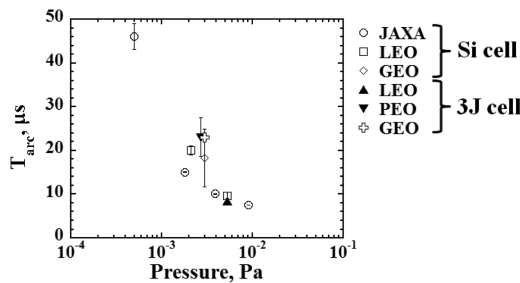| Conditions	Chamber A				LEO chamber		GEO chamber
Pressure, Pa	5.0×10^{-4}	1.8×10^{-3}	3.9×10^{-3}	9.1×10^{-3}	5.3×10^{-3}	2.1×10^{-3}	3.0×10^{-3}
T_{arc}, μs	46 ± 3.0	15 ± 0.1	10 ± 0.1	7.4 ± 0.0	9.5 ± 0.9	20 ± 1.0	18.3 ± 6.6
I_{peak}, A	10.2 ± 1.4	41.9 ± 3.3	64.1 ± 7.4	71.2 ± 25.4	36.2 ± 5.0	34.1 ± 2.0	18.3 ± 6.6
Q_{arc}, mC	0.21 ± 0.02	0.30 ± 0.01	0.32 ± 0.38	0.31 ± 0.71	0.18 ± 0.02	0.29 ± 0.05	0.21 ± 0.01
Bias voltage, V	-470	-530	-450 to -530	-400 to -480	-400	-560	-4000
N_{arc}	5	8	14	12	19	19	40

Table 4 Primary arc current characteristics of the 3J cell in the LEO chamber, PEO chamber, and GEO chamber

Conditions	LEO chamber	GEO chamber	PEO chamber
Pressure, Pa	5.3×10^{-3}	3.0×10^{-3}	2.7×10^{-3}
T_{arc}, μs	8.3 ± 0.8	23 ± 0.9	23 ± 4.4
I_{peak}, A	52.7 ± 1.4	28.7 ± 10.3	28.6 ± 2.6
Q_{arc}, mC	0.21 ± 0.04	0.20 ± 0.02	0.28 ± 0.01
Bias voltage, V	-400	-4000	-550 to -610
N_{arc}	16	5	4

threshold voltage. The other is to investigate the solar array strength against ESD, such as solar cell degradation or secondary arc. In Sec. II, it is found that the pressure changes the primary arc current waveform. A solar cell degradation test was performed on 3J cells in different charging conditions to investigate the influence of the primary arc current waveform on test results. In Sec. II, we mostly used Si solar cells as the test specimen. To be precise, the current waveform differs depending on the type of the solar cell, as the material property at the cathode spot is different. However, this difference is not very significant, as seen in Fig. 7. Because degradation of the 3J cells is easier to detect than that of the Si cells, we use 3J cells to show the effect of current waveform on the degradation.

The test was performed in the LEO chamber and GEO chamber. The test environment in the LEO chamber is 5.4×10^{-3} Pa of the pressure, 1×10^{12} m^{-3} of the plasma density, and 1 eV of the electron temperature. The test environment in the GEO chamber is the same as that listed in Table 2. To change the arc current waveform, we changed C_{ext} from 0.25 to 100 nF in the GEO chamber, and C_{ext} was changed from 50 to 500 nF in the LEO chamber. Fifteen 3J cells were used for the test.

An example of the light power-voltage characteristics of a 3J cell before and after the experiment is shown in Fig. 8. In this example, three primary arcs were observed at the solar cell edge. Two of the three primary arcs caused the degradation of Fig. 8. One arc had a peak of 39.9 A, pulse duration of 9.2 μs, and total charge of 0.19 mC, and the other had a peak of 41.9 A, pulse duration of 8.6 μs, and total charge of 0.19 mC. The maximum power before and after the experiment are defined as $P_{max_{before}}$ and $P_{max_{after}}$, respectively. Ideally, we should measure the light power-voltage characteristics after each
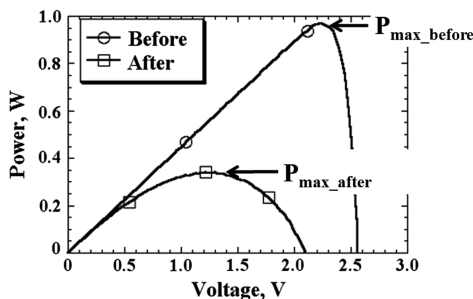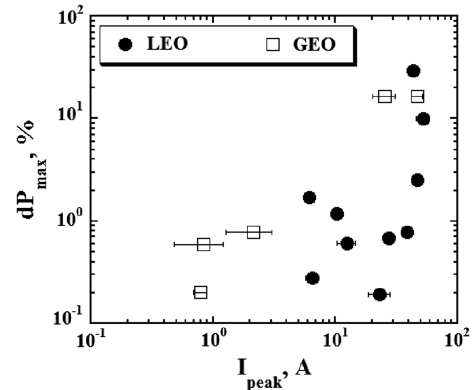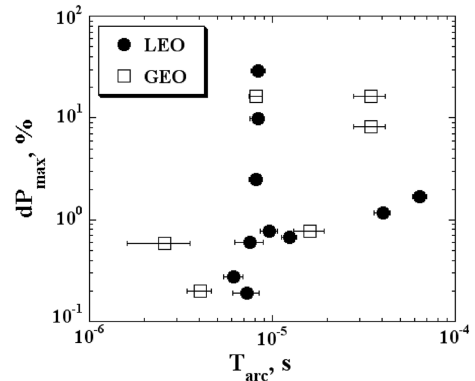
primary arc. To do this, it is necessary to irradiate the solar cell with a simulated sunlight. However, it is difficult to control the temperature of the solar cell inside the vacuum chamber. To perform the test efficiently, it is not practical to measure the light power-voltage characteristics during the test. Therefore, we defined the average reduction of P_{max} due to one primary arc as in Eq. (3):

$$dP_{max} = \frac{(P_{max_{before}} - P_{max_{after}})}{P_{max_{before}} \times N_{arc}} \times 100\% \qquad (3)$$

The relationships between I_{peak} and dP_{max} and between T_{arc} and dP_{max} are shown in Figs. 9 and 10 respectively. I_{peak} ranges from 0.8 to 53.0 A. T_{arc} ranges from 2.5 μs to 63.9 μs. In Figs. 9 and 10, each point has different Q_{arc}.

From the results of Figs. 9 and 10, the solar cell degradation is seen to have occurred in both the GEO and LEO chambers. The primary arc concentrates the energy to an area well known as the cathode spot, for which the size is much smaller than the Debye length of plasma. Therefore, whether a primary arc causes the solar cell degradation or not depends on what kind of plasma exists around the solar cell. The degradation characteristics shown in Figs. 9 and 10 depend on the solar cell type. Generally speaking, a Si solar cell is stronger than a 3J solar cell. The relationship between primary arc parameter and dP_{max} on the Si cell is reported in [10].

The power loss dP_{max} is found to increase with increase of I_{peak}, as shown in Fig. 9. From Fig. 10, we cannot see clear correlation between dP_{max} and T_{arc}. In Sec. II, we have seen that the primary arc current supplied by an external capacitance can have a different waveform under a different pressure. The higher the background pressure, the higher the peak I_{peak} becomes. Therefore, even if we use the same external circuit, the result of the solar cell degradation test may be different if the background pressure is different. What is important in the test is that we simulate the actual primary current

Fig. 7 Relationship between duration of the primary arc current and vacuum pressure; error bars indicate the standard deviation and JAXA denotes the Japan Aerospace Exploration Agency.

Fig. 8 Light current-voltage characteristics of the 3J cell.

Fig. 9 Relationship between I_{peak} and dP_{max} in different charging environments.

Fig. 10 Relationship between T_{arc} and dP_{max} in different charging environments.

waveform that would be seen in orbit. Having a capacitor alone to simulate the primary arc current should be avoided, because the background pressure affects the waveform. We need to add a mechanism to control the current supplied by the external capacitance. In other words, for the solar cell degradation test, as long as we control the primary arc current, we do not need to worry so much about the background pressure or the charging environment.

IV.   Secondary Arc Test

As the secondary arc can potentially cause catastrophic solar array failure due to the loss of power generation, a secondary arc test to check the insulation strength of the solar array is very important. To establish an international standard for the solar array ESD test, the environmental effect on the secondary arc test needs to be known. We performed the secondary arc test in a plasma environment and a high-energy electron environment to understand the environmental effect on the secondary arc sustained time.

A.   Definition of a Secondary Arc

The secondary arc is categorized into three types, as shown in Fig. 11.

1) In a nonsustained arc (NSA), a string gap is short-circuited during primary arc event.

2) In a temporary sustained arc (TSA), a string gap is short-circuited for a certain time after the primary arc event but recovers spontaneously. This type of the secondary arc causes temporary loss of output in the solar array.

3) In a permanent sustained arc (PSA), a string gap remains short-circuited permanently. This type of the secondary arc causes catastrophic solar array failure.

The criterion for determining TSA or NSA is how long the secondary arc continues from the end time of the primary arc current. We defined the end time T_{end} of a primary arc as the time when the
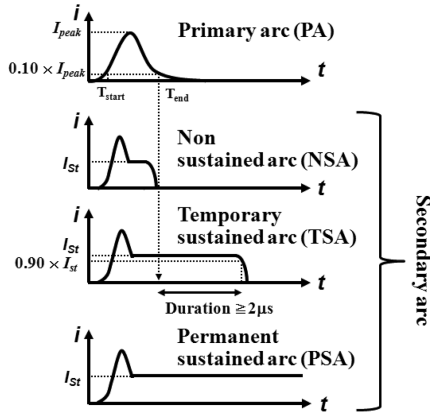
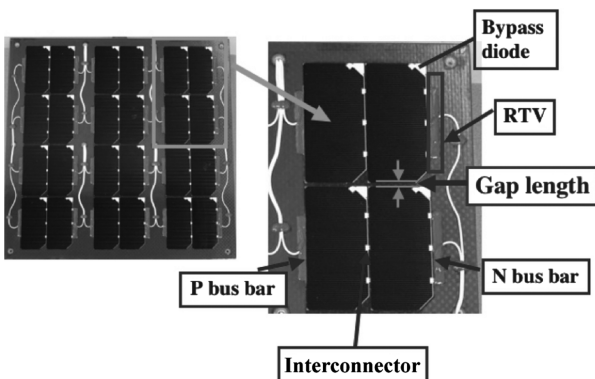current becomes 10% of its peak value. In Sec. III, the judging criteria of the end of a primary arc current was 5% of its peak value. For the degradation test, we need to precisely calculate the charge of the primary arc current. On the other hand, for the case of the secondary arc test, we need to avoid the noise to calculate a correct secondary arc sustained time. Therefore, we use the different criteria. We defined the duration of the secondary arc as the time from T_{end} to the time when the arc current becomes 90% of the string current I_{st} of the power supply. We defined a secondary arc as a NSA if the arc end is within 2 μs from T_{end} and as a TSA otherwise. This 2 μs criterion is based on our experience with distinguishing the arc current from the background oscillatory noise.

B.   Test Coupon and Discharge Circuit

The test coupon is shown in Fig. 12. The number of 3J cells on the test coupon is 24. We used four 3J cells as a group for one secondary arc test. The string gap is 1.0 mm. To prevent a primary arc anywhere except the string gap, we covered all the exposed conductive surface except the string gap, such as interconnector and bus bar, with polyimide tape.

We used the LEO and GEO chambers mentioned in Sec. II for the secondary arc test. The discharge circuit is shown in Fig. 13. The experiment condition is listed in Table 5. The pressure during the test is 2.0×10^{-4} Pa in the GEO chamber. The electron beam energy is 5 keV. The electron beam current density is 6.0–11.9 mA/m^2. The current density of this beam environment is much higher than that of a typical GEO environment to have enough arcs in a limited time. Our objective is to see whether the presence of the dense LEO-like plasma affects the secondary arc phenomena or not. In that sense, matching the beam current density to a realistic value is not
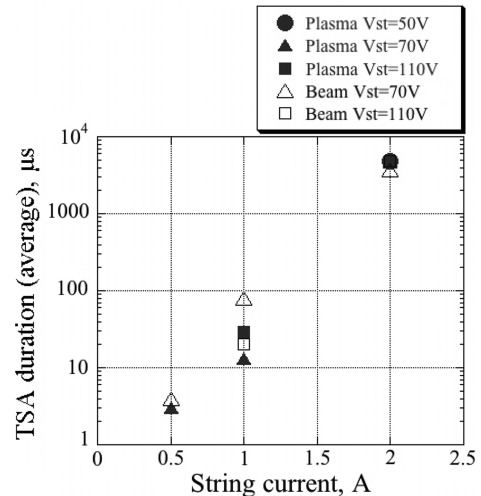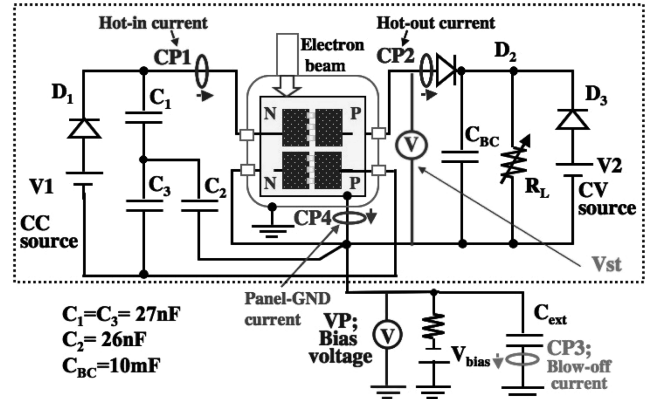

Fig. 13   Test circuit of the secondary arc test.

Fig. 11   Types of secondary arc.

Fig. 12   Solar array coupon for the secondary arc test (RTV denotes room-temperature vulcanizing).

Fig. 14   Sustained time of TSA.

Table 5 Experiment environment for the secondary arc experiment

Plasma environment		Beam environment	
Conditions	Values	Conditions	Values
Pressure, Pa	1.3×10^{-3}	Pressure, Pa	2.0×10^{-4}
Plasma density, m^{-3}	4.0×10^{11}	Beam energy, keV	5.0
Electron temperature, eV	1.0	Current density, mA/m^2	6.0–11.9

Table 6 Characteristics of the primary arc in the high-energy electron beam environment at $V_{bias} = -5$ kV and $C_{ext} = 0.3$ nF

Conditions	Minimum	Maximum	Average	Standard deviation
Peak current, A	0.2	0.5	0.3	0.1
Charge, μC	1.3	1.6	1.5	0.1
Pulse width, μs	6.9	13.1	9.6	1.6

Table 7 Characteristics of the primary arc in the plasma environment at $V_{bias} = -800$ V and $C_{ext} = 2.9$ nF

Conditions	Minimum	Maximum	Average	Standard deviation
Peak current, A	2.1	3.4	2.6	0.4
Charge, μC	3.6	4.1	3.9	0.1
Pulse width, μs	2.7	3.9	3.4	0.3

important. The pressure during the test is 1.3×10^{-3} Pa in the LEO chamber. The plasma density of the plasma source is 4.0×10^{11} m^{-3}. The electron temperature of the plasma source is 1.0–2.0 eV. We use the same discharge circuit as shown in Fig. 13 for tests in the LEO chamber and GEO chamber. The voltage supplies V_1 and V_2 simulate the power generation of the solar array. We used solar array simulator for V_1. The response time of the solar array simulator is faster than a typical commercial voltage supply. R_L is the electric load of the spacecraft. In Fig. 13, $CP1$, 2, 3, and 4 are current probes. Subtracting the waveform of $CP2$ from that of $CP1$, the secondary arc current waveform is obtained. The potential difference between the strings is measured by the differential voltage probe V_{st}. The capacitance C_{BC} (10 mF) simulates the bus capacitance of the satellite. $C1$, $C2$, and $C3$ are the capacitances equivalent to one string of the solar array, which has 50 solar cells in series [16].

The sustained duration of a TSA is an important indicator, because a TSA that sustains for a longer time can become a PSA. In the secondary arc test, we changed both the output voltage and output current (string current) of the power supplies V_1 and V_2 to compare the sustained time of the TSA in different conditions of the power supply. As the TSA creates an arc track at the string gap, we changed the string gap in each condition of the power supply to keep the same condition of the string gap as much as possible. C_{ext} is 0.3 nF and V_b is -5 kV in the high-energy electron beam environment. C_{ext} is 2.9 nF and V_b is -800 V in the plasma environment.

C. Result of the Secondary Arc Test

To investigate the dependence of the charging environment on the duration of a TSA, we changed the output voltage and output current of power supply V_1. The output voltage was 50, 70, 90, and 110 V. The output current was 0.5, 1.0, and 2.0 A. The characteristics of the primary arc listed shown in Table 6 (electron beam environment) and Table 7 (plasma environment). The number of samples was 27 for the beam environment and 22 for the plasma environment. The peak and charge of the primary arc current in the plasma environment are greater than those in the high-energy electron beam environment. However, the duration and energy of the primary arc in the high-energy electron beam environment is greater than those in the plasma environment. Primary arc energy is 4.0 mJ for the beam environment

Table 8 Statistics of duration of a TSA (μs); string voltage is 50 V

	Environment[a]									
	Plasma					Beam				
String current, A	TSA	Min	Max	Avg	Std	TSA	Min	Max	Avg	Std
0.5	No data	No data	No data	No data	No data	No data	No data	No data	No data	No data
1.0	No data	No data	No data	No data	No data	No data	No data	No data	No data	No data
2.0	1	4800.0	4800.0	4800.0	——	No data	No data	No data	No data	No data

[a]No data means that no secondary arc was observed.

Table 9 Statistics of duration of a TSA (μs); string voltage is 70 V

	Environment[a]									
	Plasma					Beam				
String current, A	TSA	Min	Max	Avg	Std	TSA	Min	Max	Avg	Std
0.5	3	2.0	3.0	2.7	1.0	1	4.0	4.0	4.0	——
1.0	10	3.0	60.0	13.0	17.0	5	15.0	184.0	78.0	67.0
2.0	N/A	N/A	N/A	N/A	N/A	4	3640.0	4830.0	1230.0	1697.0

[a]N/A means that no experiment was done.

Table 10 Statistics of duration of a TSA (μs); string voltage is 110 V[a]

	Environment									
	Plasma					Beam				
String current, A	TSA	Min	Max	Avg	Std	TSA	Min	Max	Avg	Std
0.5	No data	No data	No data	No data	No data	No data	No data	No data	No data	No data
1.0	19	3.0	140.0	29.0	38.0	7	3.0	40.0	20.0	18.0
2.0	6	3720.0	4820.0	4638.0	450.0	2	4830.0	4830.0	4830.0	0.0

[a]No data means that no secondary arc was observed.

and 0.9 mJ for the plasma environment. The average duration of TSA is shown in Fig. 14. The statistics of TSA duration are listed in Tables 8–10. In the tables, the numbers larger than 4800 μs mean that the true duration was unknown, because the waveform was beyond the horizontal scale of the oscilloscope. There is no difference in the TSA duration between the plasma environment and the electron beam environment, as shown in Fig. 14 and Tables 8–10. The TSA duration increases exponentially with the string current. Although the characteristics of the primary arc are different between the two environments, the TSA duration increases with the string current for both environments. Therefore, the primary arc current waveform and the charging environment do not affect the secondary arc test results in terms of the TSA duration. It is thus not necessary to control the environment in the secondary arc test to check the PSA inception.

Once the gap is short-circuited by the primary arc plasma, the current goes through the secondary arc plasma. How long the secondary arc plasma can last depends mostly on how much current flows through the secondary arc plasma, not on how the primary arc plasma was generated. It should be noted that whether a primary arc can become a NSA or TSA may still depend on how the primary arc plasma was generated. If the test purpose is to check the occurrence of the secondary arc in general, not confined to the PSA inception, it is advised to make the primary arc flight-representative.

V. Primary Arc Current Waveform Control Circuit

The primary arc current waveform affects the solar cell degradation test results. Therefore, we have to control the peak, the duration, and the energy of the primary arc current. The discharge circuits to control the primary arc current waveform are shown in Figs. 15 and 16. Toyoda et al. [17] and Nomura et al. [18] designed these discharge circuits. In the discharge circuit in Fig. 15, termed the LCR discharge circuit, a resistance (R) and an inductance (L) are connected in series with the capacitance C_{ext} in the discharge circuit shown in Fig. 3. The primary arc current waveform using the circuit of Fig. 15 is shown in Fig. 17, in which the bias voltage V_b was 400 V and the LEO chamber was filled with a Xe plasma of 1×10^{-2} m^{-3}
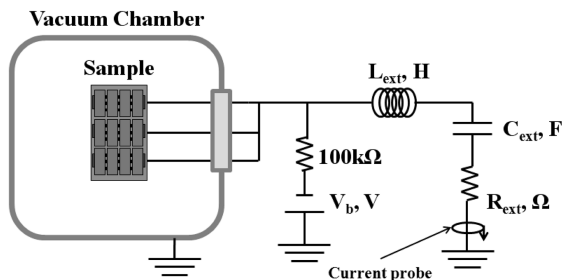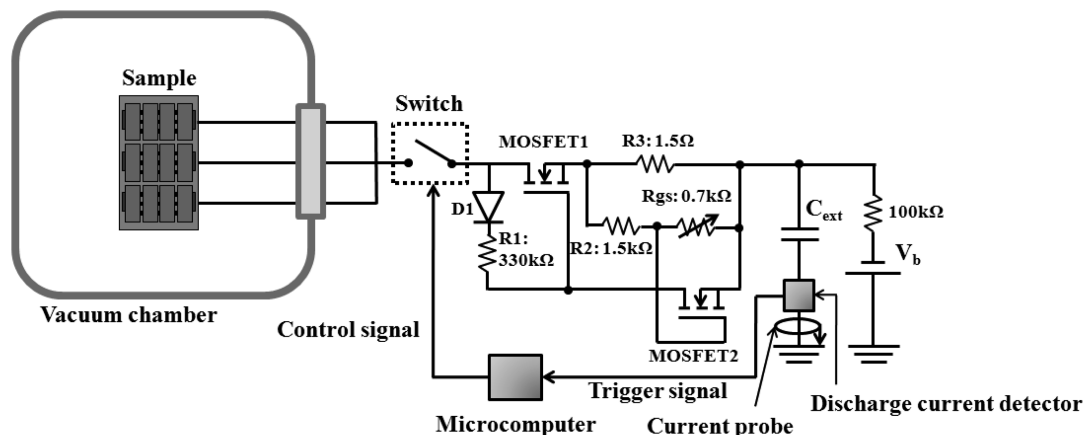

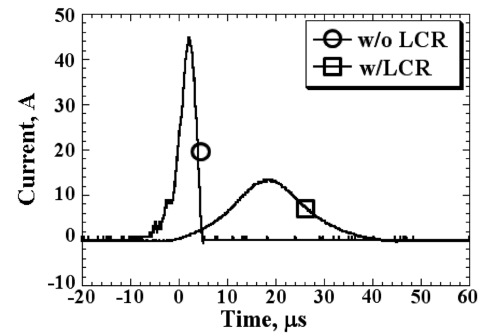Fig. 15 Discharge experiment circuit with the LCR circuit.

Fig. 17 Primary arc current waveform in the case of discharge circuit with LCR and without LCR.
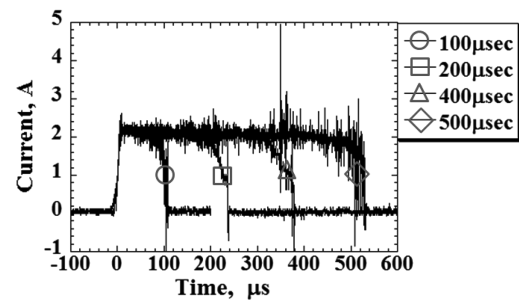

Fig. 18 Primary arc current waveforms produced by the discharge circuit with the MOSFET circuit.

density and 1 eV density under the background pressure of 5.3×10^{-3} Pa. The current was measured by a current probe. Although the capacitance is fixed at 500 nF, we can control the primary arc current waveform by changing the resistance and inductance. In Fig. 17, the duration of the primary arc was changed from 10 to 35 μs by adding the inductance of 270 μH and the resistance of 4Ω.

In the discharge circuit shown in Fig. 16, MOSFET, a microprocessor, and a current detector are attached in the discharge circuit shown in Fig. 3. The current detector sends a signal to the microprocessor when it detects a primary arc. The microprocessor sends a switch-off signal to MOSFET after waiting for a given time. When MOSFET receives the signal from the microprocessor, MOSFET changes the state from on to off, forcing the primary arc current to stop. The primary arc current level is controlled by R_{gs}. The primary arc current waveforms with the discharge circuit of Fig. 16 are shown in Fig. 18. The primary arc current level was set to 2 A. The duration of the primary arc is changed from 100 to 500 μs. This discharge circuit is able to change the primary arc duration on the order of hundreds of microseconds. The discharge circuits, which are shown in Figs. 15 and 16, prove that the solar cell degradation test is possible

Fig. 16 Discharge experiment circuit with the MOSFET circuit.

without rigorous restriction on the pressure and the charging environment.

VI. Conclusions

In the present paper, we have investigated dependence of the primary arc waveform on the chamber pressure and the charging environment in the solar array ESD test. The primary arc current waveform mostly depends on the chamber pressure, because the background gas determines the resistance between cathode spot and chamber wall.

The outcome of the ESD test, especially the solar cell degradation test, depends on the primary arc current waveform. The higher the peak, the more degradation occurs, due to a single pulse of ESD. The important aspect of ESD test is not to maintain good vacuum, although that is always desirable, but to simulate the primary arc current waveform in orbit as closely as possible. Therefore, a pulse-forming circuit should be attached to the external capacitance, which simulates the solar array coverglass capacitance. We have introduced examples of a pulse-forming circuit. One uses a series of MOSFET switches controlled by a microcomputer. Another one uses an inductance and a resistance. As long as we apply the pulse-forming circuit for the solar cell degradation test, a background pressure is not an important factor. The question here pertains to the flight-representative current waveform. Because there has been no on-orbit measurement of the discharge waveform, we have to assume a discharge waveform in orbit. Fortunately, there have been several ground experiments carried out independently to investigate the flight-representative waveform that can serve as the basis of the physical model to assume the waveform. In the future, we should find an opportunity to measure the primary arc current waveform in orbit.

The secondary arc test has been done in both the plasma environment and the electron beam environment. Once a primary arc becomes a secondary arc, its duration is mostly determined by the current available from the power supply, regardless of the charging environment or the primary arc current waveform. The secondary arc duration has an exponential dependence on the current from the power supply. If the test purpose is to study a permanent sustained arc or a very long temporary sustained arc that is devastating enough for a given solar array design, we should pay the most attention to making the current from the power supply as flight-representative as possible. The external circuit layout has a significant impact on the test result. Finding a suitable circuit layout for the secondary arc test is one of the issues to be investigated further.

If the test purpose is to check the occurrence of the secondary arc in general and is not confined to the permanent sustained arc inception (for example, characterizing the probability of a primary arc becoming a secondary arc), the effect of the primary arc current waveform is still unknown. That point should be investigated further in the future. Until then, it is safe to use a flight-representative charging environment and to make the primary arc current flight-representative.

Acknowledgments

References

[1] Katz, I., Davis, V. A., and Snyder, D. B., "Mechanism for Spacecraft Charging Initiated Destruction of the Solar Arrays in GEO," 36th Aerospace Sciences Meeting, AIAA Paper 98-1002, 1998.

[2] Cho, M., "Status of ISO Standardization Efforts of the Solar Panel ESD Test Methods," *10th Spacecraft Charging Technology Conference on Disk* [CD-ROM], Japan Aerospace Exploration Agency, Tsukuba, Japan, June, 2007.

[3] Hastings, D., and Garrett, H., *Spacecraft Environment Interactions*, Cambridge Univ. Press, New York, 1996, pp. 142–198.

[4] Okumura, T., Masui, H., Toyoda, K., Imaizumi, M., and Cho, M., "Degradation of Electric Performance Due to Electrostatic Discharge on Silicon Solar Cell for Space," *Journal of the Japan Society for Aeronautical and Space Sciences*, Vol. 55, No. 647, 2007, pp. 590–596.
doi:10.2322/jjsass.55.590

[5] Okumura, T., Hosoda, S., Kim, J., Kagawa, H., and Cho, M., "Degradation of the Solar Cell Electric Performance Due to Arcing in the LEO Plasma Environment," *9th Spacecraft Charging Technology Conference on Disk* [CD-ROM], Japan Aerospace Exploration Agency, Tsukuba, Japan, Apr. 2007.

[6] Cho, M., Ramasamy, R., Matsumoto, T., Toyoda, K., Nozaki, Y., and Takahashi, M., "Laboratory Tests on 110 V Solar Arrays in a Simulated Geosynchronous Orbit Environment," *Journal of Spacecraft and Rockets*, Vol. 40, No. 2, 2003, pp. 211–220.
doi:10.2514/2.3955

[7] Cho, M., Kim, J., Hosoda, S., Nozaki, Y., Miura, T., and Iwata, T., "Electrostatic Discharge Ground Test of a Polar Orbit Satellite Solar Panel," *IEEE Transactions on Plasma Science*, Vol. 34, No. 5, 2006, pp. 2011–2030.
doi:10.1109/TPS.2006.881935

[8] Matéo-Vélez, J.-C., Inguimbert, V., Sarrail, D., Levy, L., Boulay, F., Roussel, J.-F., Laffornt, E., and Payan, D., "Degradation of the Solar Cell by ESDs," *10th Spacecraft Charging Technology Conference on Disk* [CD-ROM], Japan Aerospace Exploration Agency, Tsukuba, Japan, June 2007.

[9] Vayner, B., Furguson, D., and Galofaro, J., "Detrimental Effect of Arcing on Solar Array Surfaces," *10th Spacecraft Charging Technology Conference on Disk* [CD-ROM], Japan Aerospace Exploration Agency, Tsukuba, Japan, June 2007.

[10] Okumura, T., Ninomiya, S., Masui, H., Toyoda, K., Imaizumi, M., and Cho, M., "Solar Cell Degradation Due to ESD for International Standardization of the Solar Array ESD Test," *10th Spacecraft Charging Technology Conference on Disk* [CD-ROM], Japan Aerospace Exploration Agency, Tsukuba, Japan, June 2007.

[11] Gaillot, L., Fille, M.-L., and Lévy, L., "Secondary Arcs on Solar Array —Test Results on EMAG2," *9th Spacecraft Charging Technology Conference on Disk* [CD-ROM], Japan Aerospace Exploration Agency, Tsukuba, Japan, Apr. 2005.

[12] Amorim, M., and Payan, D., "Electrostatic Discharges on a 1M2 Solar Array Coupon—Influence of the Energy Stored on Coverglass on Flashover Current," *9th Spacecraft Charging Technology Conference on Disk* [CD-ROM], Japan Aerospace Exploration Agency, Tsukuba Japan, Apr. 2005.

[13] Masui, H., Toyoda, K., and Cho, M., "Electrostatic Discharge Plasma Propagation Velocity on Solar Panel in Simulated Geosynchronous Environment," *10th Spacecraft Charging Technology Conference on Disk* [CD-ROM], Japan Aerospace Exploration Agency, Tsukuba, Japan, June 2007.

[14] Leung, P., "Plasma Phenomena Associated with Solar Array Discharges and Their Role in Scaling Coupon Test Results to a Full Panel," 40th Aerospace Sciences Meeting, Reno, NV, AIAA Paper 2002-0628, Jan. 2002.

[15] Mashidori, H., Nitta, K., Kawakita, S., Harada, J., Miki, Y., Shinohara, S., and Toyoda, K., "Preliminary ESD Ground Tests Using a Large-Scale Solar Array," *10th Spacecraft Charging Technology Conference on Disk* [CD-ROM], Japan Aerospace Exploration Agency, Tsukuba, Japan, June 2007.

[16] Payan, D., Schwander, D., and Catani, J. P., "Risks of Low Voltage Arcs Sustained by the Photovoltaic Power of a Satellite During an Electrostatic Discharge Solar Arrays Dynamic Simulator," *7th Spacecraft Charging Technology Conference on Disk* [CD-ROM], ESA, Noordwijk, The Netherlands, 2001.

[17] Toyoda, K., Okumura, T., Hosoda, S., and Cho, M., "Degradation of High Voltage Solar Array Due to Arcing in the LEO Plasma Environment," *Journal of Spacecraft and Rockets*, Vol. 42, No. 5, 2005, pp. 947–953.
doi:10.2514/1.11602

[18] Nomura, M., Masui, H., Toyoda, K., and Cho, M., "Development of Flashover Current Simulation Circuit for ESD Ground Test of the Solar Array Paddle," *10th Spacecraft Charging Technology Conference on Disk* [CD-ROM], Japan Aerospace Exploration Agency, Tsukuba, Japan, 18–21 June 2007.

A. Ketsdever
Associate Editor